High concentration methanol fuel cells: Design and theory

Christian E. Shaffer, Chao-Yang Wang*

Department of Mechanical and Nuclear Engineering, and Electrochemical Engine Center (ECEC), The Pennsylvania State University, University Park, PA 16802, United States

ABSTRACT

Use of highly concentrated methanol fuel is required for direct methanol fuel cells (DMFCs) to compete with the energy density of Li-ion batteries. Because one mole of H_2O is needed to oxidize one mole of methanol (CH_3OH) in the anode, low water crossover to the cathode or even water back flow from the cathode into the anode is a prerequisite for using highly concentrated methanol. It has previously been demonstrated that low or negative water crossover can be realized by the incorporation of a low-α membrane electrode assembly (MEA), which is essentially an MEA designed for optimal water management, using, e.g. hydrophobic anode and cathode microporous layers (aMPL and cMPL). In this paper we extend the low-α MEA concept to include an anode transport barrier (aTB) between the backing layer and hydrophobic aMPL. The main role of the aTB is to act as a barrier to CH_3OH and H_2O diffusion between a water-rich anode catalyst layer (aCL) and a methanol-rich fuel feed. The primary role of the hydrophobic aMPL in this MEA is to facilitate a low (or negative) water crossover to the cathode. Using a previously developed 1D, two-phase DMFC model, we show that this novel design yields a cell with low methanol crossover (i.e. high fuel efficiency, ~80%, at a typical operating current density of ~80–90% of the cell limiting current density), while directly feeding high concentration methanol fuel into the anode. The physics of how the aTB and aMPL work together to accomplish this is fully elucidated. We further show that a thicker, more hydrophilic, more permeable aTB, and thicker, more hydrophobic, and less permeable aMPL are most effective in accomplishing low CH_3OH and H_2O crossover.
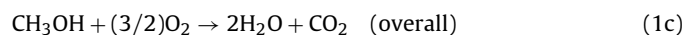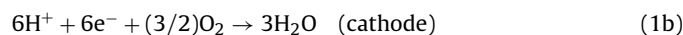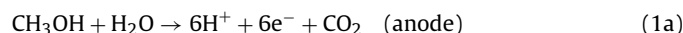
© 2010 Elsevier B.V. All rights reserved.

1. Introduction

Given that methanol fuel is roughly four times more energy dense than Li-ion battery materials (~4800 Wh l^{-1} vs. ~1200 Wh l^{-1} [1]), there is great promise for direct methanol fuel cells (DMFCs) to replace Li-ion batteries as the power source of choice in mobile devices [1–8]. However, difficulties in being able to directly feed highly concentrated fuel, along with low energy conversion efficiency (~25% [4]), have plagued DMFC technology, and yielded designs with practical energy densities far below the theoretical value for methanol (CH_3OH). Therefore, in order to compete with Li-ion batteries, advanced DMFCs must first be designed that realize a greater practical energy density (Wh l^{-1}) [3,4,8] by efficiently and directly using highly concentrated methanol fuel [6–8].

In order to use highly concentrated methanol fuel, water management becomes a key issue [6–18]. This point is highlighted by analyzing the basic half-cell and overall reactions for a DMFC, as given by Eq. (1). In the anode catalyst layer (aCL), one mole of H_2O

reacts with one mole of CH_3OH in the methanol oxidation reaction (MOR), equation (1a). In the cathode catalyst layer (cCL), H_2O is produced by the oxygen reduction reaction (ORR), Eq. (1b), and by crossed-over CH_3OH in the overall reaction, Eq. (1c):

$$CH_3OH + H_2O \rightarrow 6H^+ + 6e^- + CO_2 \quad \text{(anode)} \tag{1a}$$

$$6H^+ + 6e^- + (3/2)O_2 \rightarrow 3H_2O \quad \text{(cathode)} \tag{1b}$$

$$CH_3OH + (3/2)O_2 \rightarrow 2H_2O + CO_2 \quad \text{(overall)} \tag{1c}$$

The 1:1 stoichiometric ratio of $CH_3OH:H_2O$ for the aCL MOR is the reason that water management in DMFCs is so important for the use of high concentration methanol fuel. As highlighted by Fig. 1, in order to have a sufficient source of H_2O at steady-state and use all CH_3OH and H_2O carried in the DMFC system, a high concentration methanol fuel cell (HC-MFC) must have a low rate of water crossover to the cathode, as fully described by Lu et al. [6], Liu et al. [7], Wang and Liu [8], and Shaffer and Wang [10–13]. In fact, we see from Fig. 1 that for fuel concentration above ~17–18 M we must have a back flow of H_2O, i.e. $\alpha < 0$. Note that α is the net water transport coefficient – the net water flux across the membrane normalized by the protonic flux – and MCO is the methanol crossover ratio—the fraction of the total methanol used that crosses

* Corresponding author at: Department of Mechanical Engineering, The Pennsylvania State University, 301c Reber Bldg, University Park, PA 16802, United States. Tel.: +1 814 863 4762; fax: +1 814 863 4848.
E-mail address: cxw31@psu.edu (C.-Y. Wang).

Nomenclature

Acronyms and abbreviations

aBL	anode backing layer
aCL	anode catalyst layer
aMPL	anode microporous layer
aTB	anode transport barrier
cBL	cathode backing layer
cCL	cathode catalyst layer
cMPL	cathode microporous layer
CH_3OH	methanol
diff	diffusion
DMFC	direct methanol fuel cell
EOD	electroosmotic drag
HC-MFC	high concentration methanol fuel cell
HP	hydraulic pressure
MEA	membrane electrode assembly
Mem	membrane
MOR	methanol oxidation reaction
MPL	microporous layer
ORR	oxygen reduction reaction

Symbols

α	net water transport coefficient
$D_{\mathrm{eff},k}^{\psi_1,\psi_2}$	effective diffusivity of species ψ_1 in ψ_2 in phase k
$D_k^{\psi_1,\psi_2}$	molecular diffusivity of species ψ_1 in ψ_2 in phase k
D_{Mem}^{ψ}	membrane diffusivity of species ψ
δ_j	thickness of layer j
ε_j	porosity of layer j
F	Faraday's constant
η_{fuel}	fuel efficiency
i	cell current density
i_{xover}	crossover current density
J	Leverett function
k_{rl}	relative liquid-phase permeability
K_j	permeability of layer j
λ	ionomer water content
MCO	methanol crossover ratio
M_k	molecular weight of phase k
μ_k	viscosity of phase k
n	Bruggeman exponent
n_{d}^{ψ}	electroosmotic drag coefficient of species ψ
N_{l}	total flux of liquid phase
N_{l}^{ψ}	flux of species ψ in the liquid phase
N_{Mem}^{ψ}	membrane flux of species ψ
θ_j	contact angle of layer j
ρ_{k}	density of phase k
s	liquid saturation (i.e. liquid volume fraction in pore space)
σ	surface tension
x	through-plane coordinate axis
X_{l}^{ψ}	mole fraction of species ψ in the liquid phase

Fig. 1. Methanol fuel concentration vs. α required at steady-state operation for full use of CH_3OH and H_2O carried by the DMFC system; assumes no external water management; $T = 60\,^{\circ}C$ in this plot.

H_2O. An alternative explanation is that a point above or below a given curve in Fig. 1 indicates a DMFC system operating with an excess of either CH_3OH or H_2O, and thereby not making the most efficient use of the volume of the DMFC system. This point is further highlighted by looking at Fig. 2, which shows that ~ 17 M fuel has a 1:1 molar ratio of CH_3OH:H_2O. For $\alpha = 0$ and MCO = 0, this implies that at steady-state, the cell will simultaneously run short of CH_3OH and H_2O using ~ 17 M fuel.

It is important to point out that typical DMFCs not utilizing low-α MEA technology generally have $\alpha \sim 2$–3, at common operating current densities. For this condition, we see from Fig. 1 that a maximum of only ~ 3–5 M methanol fuel can be used, a point made by Lu et al. [6], Liu et al. [7], and Wang and Liu [8]. In effort to boost the potential for using highly concentrated methanol fuel, the low-α MEA design was first proposed by Lim and Wang [19] and has since been implemented in various forms by a number of researchers [6–8,10–18,20–23]. Lu et al. [6] and Liu et al. [7] implemented a low-α MEA with thin Nafion® 112 membrane along with hydrophobic

the membrane and reacts in the cathode:

$$\alpha = N_{\mathrm{Mem}}^{H_2O}\left(\frac{F}{i}\right) \qquad (2)$$

$$MCO = \frac{i_{xover}}{i + i_{xover}} = 1 - \eta_{\mathrm{fuel}} \qquad (3)$$

A point lying above a given MCO curve in Fig. 1 implies that a cell operating at the specified MCO will run short of H_2O before CH_3OH, as there will be an insufficient source of H_2O entering the aCL; a point lying below a given curve means a shortage of CH_3OH before
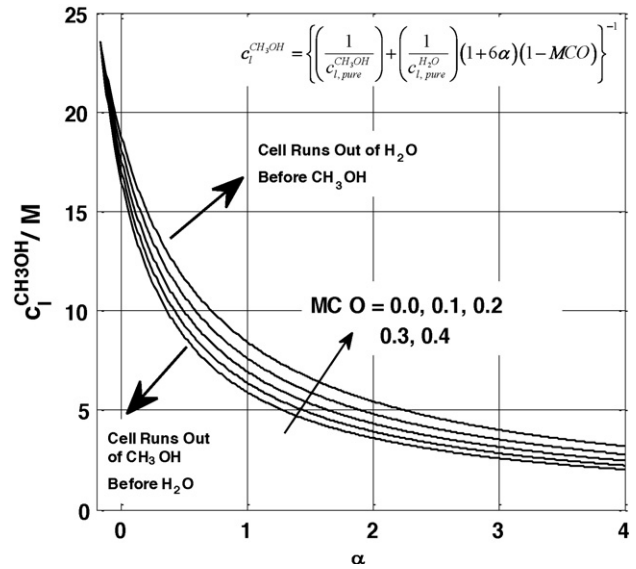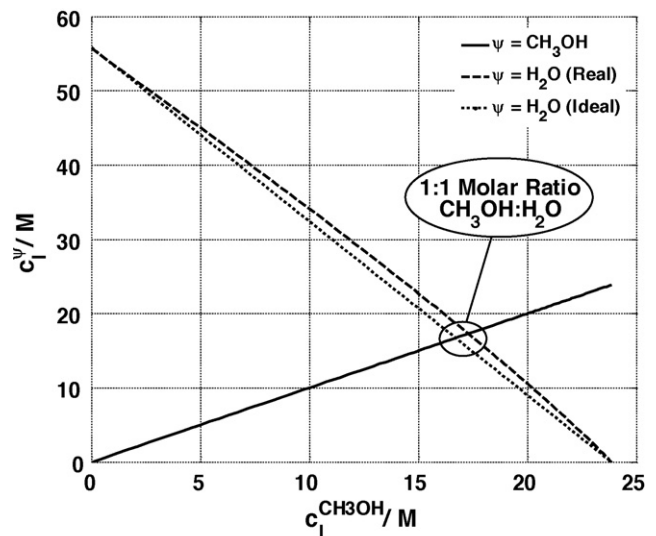

Fig. 2. Liquid methanol and water concentrations for ideal and real binary liquid solution. Real solution data adopted from [36]; $T = 25\,^{\circ}C$ in this plot.

anode and cathode microporous layers (MPLs). As a benchmark of sorts for this technology, the authors [6,7] demonstrated that they could reduce water crossover to $\alpha \sim 0.6$–0.8 at 60 °C while still maintaining a high fuel efficiency ($\sim$80–90%), cell voltage ($\sim$0.4 V), and power density ($\sim$60 mW cm^{-2}). More recently, it was further shown that α can be lowered to -0.7 at 60 °C and similar conditions [15,16].

Traditionally it has been hypothesized that the hydrophobic cathode microporous layer (cMPL) in the low-α MEA design is primarily responsible for reducing α [4,18,24]; this reduction is attributed to an increase in the liquid saturation in the cCL, forcing a back flow of water to the anode. Recently, however, Liu [14,15] discovered that a hydrophobic aMPL plays an even more significant role in reducing α, a finding which has subsequently been confirmed by Park et al. [23]. For example, using two otherwise identical Nafion® 112-based MEAs with and without hydrophobic aMPL, Liu [14,15] demonstrated $\alpha \sim 0.3$ and $\alpha \sim 1.2$, respectively, at an operating current density of 150 mA cm^{-2}. A theory of how the hydrophobic aMPL causes this significant drop in α has been presented by Liu and Wang [14,15], and further developed by Shaffer and Wang [10–13]. This theory [10–15] conjectures that the aMPL reduces α by lowering the liquid saturation level in the aCL, ultimately facilitating an increased back flow of H$_2$O across the membrane from cathode to anode.

With the notable exception of Refs. [8,17,18], the low-α MEA literature to date has generally concentrated on ways to reduce α – a prerequisite for direct use of high concentration fuel – while still using relatively low concentration methanol fuel ($\sim$2–3 M). In this work we extend the low-α MEA concept and present a novel MEA design with hydrophobic aMPL and additional anode transport barrier (aTB) between anode backing layer (aBL) and aMPL. The primary role of the aMPL in this design is to minimize the amount of water that crosses through the membrane to the cathode (i.e. reduce α, possibly even creating a net back-flux of water from cathode to anode); the primary role of the aTB is to act as an obstruction to methanol and water diffusion between the flow channel and the aCL. As such, the aMPL and aTB work in concert with one another to yield an MEA that realizes low α and low MCO while using highly concentrated methanol fuel. In this paper, our novel MEA design is described in detail, but more importantly, the physics of how such design is successful is elucidated utilizing a 1D, two-phase transport model described previously in Refs. [10,11].

2. Model

The details of the 1D model used in this study are given in Refs. [10,11]. Here we give a brief overview of the model, which is an extension of a 1D model previously presented by Liu [25]. Notable major expansions beyond the work [25] include: (1) incorporation of a saturation jump model; (2) incorporation of a cathode mixed potential electrochemistry model; (3) explicit treatment of CLs as zones of finite thickness rather than infinitely thin interfaces; (4) incorporation of MPL and aTB models; and (5) the ability to model the transition between a single- and a two-phase region.

The geometry of the 1D DMFC model is shown in Fig. 3. Here, the distinct regions of the aBL, aTB, aMPL, aCL, membrane (Mem), cCL, cMPL, and cathode backing layer (cBL) are illustrated. The model makes the following major assumptions:

- Steady-state.
- Isothermal.
- In all two-phase regions, there exists thermodynamic equilibrium between the liquid and gas phases.
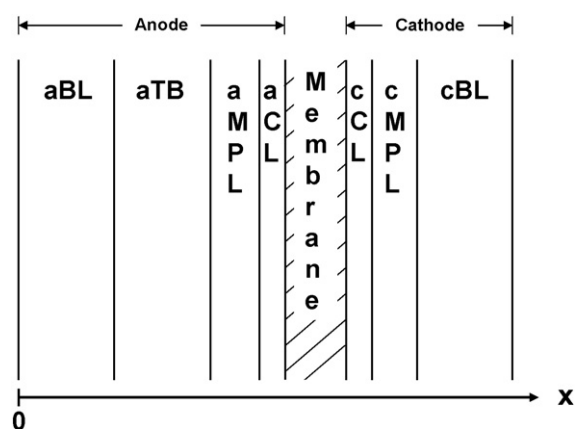- Gas-phase pressure assumed uniform over the entire anode and cathode.

Fig. 3. Geometry of 1D DMFC model.

The baseline parameters for the cell simulated in this study are given in Table 1, while Table 2 lists other important modeling parameters and correlations used.

The total species fluxes in the anode regions are determined by the current density as related to the MOR, Eq. (1a), assuming a uniform reaction rate in the aCL, and by accounting for the methanol and water membrane crossover. On the cathode side of the cell, the species fluxes are coupled with the cathode potential based on the detailed reaction mechanism of Liu and Wang [21]. The membrane transport model is a resistance-type model for both water and methanol crossover. The water crossover is determined by electroosmotic drag (EOD), diffusion (diff), and hydraulic permeation (HP), while the methanol crossover is determined by EOD and diffusion components.

The liquid- and gas-phase transport models are based on the Maxwell–Stefan equations. The crossed-over methanol in the cCL is explicitly accounted for in the transport model and by implementation of the detailed reaction mechanism given by Liu and Wang [21]. To account for the capillary-induced liquid flow in the porous media, we follow the theory presented in detail by Pasaogullari and Wang [24,26], and Nam and Kaviany [27], which uses Darcy's law to model two-phase flow through the porous media. This model allows us to fully account for the varying liquid saturation in the

Table 1
Baseline cell properties and simulation parameters.

Parameter	Value	Notes
δ_{BL} (μm)	260	Anode and cathode
δ_{aTB} (μm)	260	
δ_{MPL} (μm)	20	Anode and cathode, if present
δ_{CL} (μm)	15	Anode and cathode
δ_{Mem} (μm)	50	Nafion® 112
ε_{BL}, ε_{CL}	0.6	Anode and cathode
ε_{aTB}	0.25	
ε_{MPL}	0.4	Anode and cathode
K_{BL} (m^2)	1.0×10^{-14}	Anode and cathode
K_{aTB} (m^2)	1.0×10^{-14}	
K_{MPL} (m^2)	2.0×10^{-15}	Anode and cathode
K_{CL} (m^2)	3.6×10^{-16}	Anode and cathode
K_{Mem} (m^2)	4.0×10^{-20}	
θ_{BL} (°)	110	Anode and cathode
θ_{aTB} (°)	120	
θ_{MPL} (°)	120	Anode and cathode
θ_{CL} (°)	96	Anode and cathode
Anode stoichiometry	2.0 at 150 mA cm^{-2}	
Cathode stoichiometry	2.0 at 150 mA cm^{-2}	
$c_0^{CH_3OH}$ (M)	10	Anode flow channel inlet methanol concentration
T (°C)	60	Cell temperature

Table 2
Model parameter correlations, values, and sources.

Correlation or value	Description	Comment
$k_{rl} = s^4$	Liquid-phase relative permeability.	Ref. [28].
$D_g^{CH_3OH,H_2O} = D_g^{CH_3OH,CO_2} = 1.96 \times 10^{-5} \left(\frac{T}{328.15\,K} \right)^{1.823} \frac{1.013 \times 10^5\,Pa}{p}$ m^2 s^{-1}	Gas CH_3OH, H_2O and CH_3OH, CO_2 diffusivity.	Chapman Enskog theory for p, T dependence; reference value from [29] for air–CH_3OH, approximated same for CH_3OH, H_2O and CH_3OH, CO_2.
$D_g^{H_2O,CO_2} = 2.01 \times 10^{-5} \left(\frac{T}{307\,K} \right)^{1.823} \frac{1.013 \times 10^5\,Pa}{p}$ m^2 s^{-1}	Gas H_2O, CO_2 diffusivity.	Chapman–Enskog theory for p, T dependence; reference diffusivity from [30].
$D_g^{O_2} = 3.57 \times 10^{-5} \left(\frac{T}{352\,K} \right)^{1.823} \frac{1.013 \times 10^5\,Pa}{p}$ m^2 s^{-1}	Gas O_2 diffusivity.	Chapman–Enskog theory for p, T dependence; reference diffusivity from [30] for O_2, H_2O.
$D_l^{CH_3OH,H_2O} = 1.4 \times 10^{-9} \left[\frac{647.3 - 298.15\,K}{647.3\,K - T} \right]^6$ m^2 s^{-1}	Liquid CH_3OH diffusivity.	T dependence from [30]; reference value from [31] for dilute CH_3OH solution.
$\lambda = \begin{cases} 22 & (s > 0.3) \\ 14 + 8s/0.3 & (s \leq 0.3) \\ 0.043 + 17.81RH - 39.85RH^2 + 36.0RH^3 & \text{(vapor)} \end{cases}$	Nafion® membrane water content.	Liquid assumed interpolation, upper and lower values from [32]; vapor from [33].
$D_{Mem}^{CH_3OH} = 1.5 \times 10^{-10} \exp \left[2416 \left(\frac{1}{303\,K} - \frac{1}{T} \right) \right]$ m^2 s^{-1}	Nafion® membrane CH_3OH diffusivity.	T dependence taken from [33] for H_2O transport in Nafion® with reference value experimentally calibrated at ECEC.
$D_{Mem}^{H_2O} = 4.80 \times 10^{-11} \exp \left[2416 \left(\frac{1}{303\,K} - \frac{1}{T} \right) \right]$ m^2 s^{-1}	Nafion® membrane H_2O diffusivity.	T dependence taken from [33] with reference value calibrated at ECEC.
$n_d^{H_2O} = \begin{cases} \left[\frac{\lambda - 14}{8} \right] (n_{d,ref}^{H_2O} - 1) + 1 & \text{for } \lambda \geq 14 \\ 1 & \text{for } \lambda < 14 \end{cases}$	H_2O EOD coefficient.	Interpolation assumed; upper and lower values from [4] and [34].
$n_{d,ref}^{H_2O} = 1.6767 + 0.0155(T - 273) + 8.9074 \times 10^{-5}(T - 273)^2$	H_2O reference EOD coefficient for membrane in equilibrium with liquid H_2O.	From Ref. [4].
$n_d^{CH_3OH} = n_d^{H_2O} \frac{c_l^{CH_3OH}}{c_{t,l}}$	CH_3OH drag coefficient.	Assumed similar to Ref. [35].
$n = 2.1$	Bruggeman exponent	Assumed.

distinct layers of the diffusion media, which is critically important in being able to properly model the water transport across the membrane.

3. Results and discussion

3.1. Roles of aTB and aMPL

Before jumping into results, it is instructive to look into the nature of CH_3OH and H_2O transport in the liquid phase on the anode side of the cell, where capillary action acts to transport the mixture from the flow channel to the catalyst layer. Written generically for a species, ψ, with X_l^ψ denoting its liquid mole fraction, the flux of a given species in the liquid phase can be represented by convection and diffusion components:

$$N_l^\psi = X_l^\psi N_l + j_l^\psi \tag{4}$$

Due to the binary nature of the methanol water mixture (negligible dissolved CO_2 concentration), two things are of note:

(1) The concentration gradients of CH_3OH and H_2O must be in opposite directions of one another, i.e. as the concentration of one species increases, that of the other species must necessarily decrease, as clearly illustrated by Fig. 2.
(2) The *diffusion* flux of a species must be proportional to the negative of its concentration gradient, i.e. Fick's law is valid.

With this concept in mind, we now look at Fig. 4, which illustrates the liquid methanol and H_2O concentration profiles at 175 mA cm^{-2} for the baseline cell and the same cell without the aTB present. Here we see that in the anode transport barrier (0.26 mm < x < 0.52 mm) there is a large gradient in both liquid

CH_3OH and H_2O concentrations. This implies that the anode transport barrier poses an obstruction to methanol diffusion from the flow channel towards the aCL and H_2O back-diffusion in the opposite direction. Thus, the aTB facilitates a water-rich aCL, thereby allowing us to use high concentration methanol fuel while still realizing a low MCO (i.e. high fuel efficiency). This point is illustrated in Fig. 5, which shows the simulated MCO vs. current density for the baseline cell and the same cell without the aTB; here, using
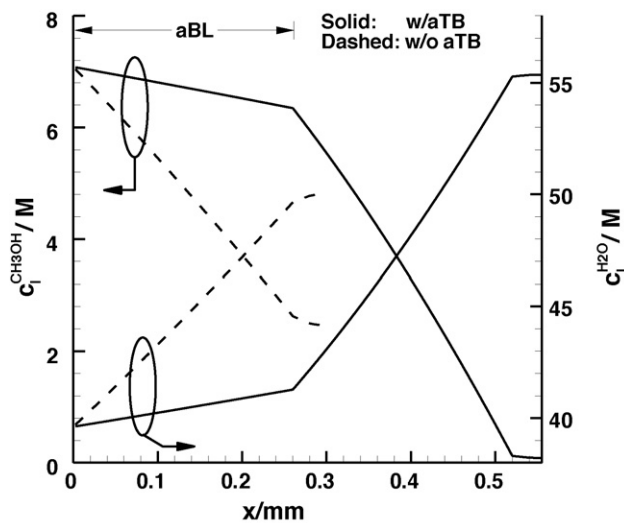

Fig. 4. Liquid CH_3OH and H_2O concentration profiles with and without aTB; aMPL present. Note that without aTB present, the aMPL is at (0.26 mm < x < 0.28 mm) and the aCL is at (0.28 mm < x < 0.295 mm); i = 175 mA cm^{-2}.
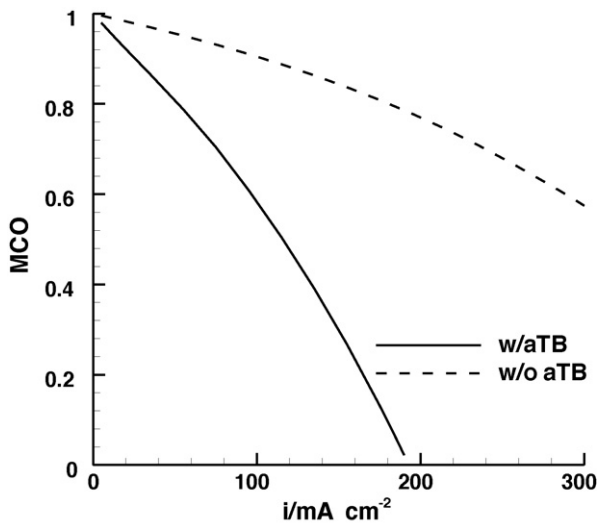
Fig. 5. MCO vs. current density with and without aTB; aMPL present.

10 M fuel, we see that, roughly, MCO < 0.3 for i > 150 mA cm^{-2} with aTB present. Analyzing the membrane methanol transport equation used in the 1D model (see Shaffer and Wang [10,11] for details) gives further physical insight into why a lower MCO is realized with lower methanol concentration in the aCL:

$$N_{\text{Mem}}^{\text{CH}_3\text{OH}} = n_{\text{d}}^{\text{CH}_3\text{OH}} \left(\frac{i}{F} \right) + D_{\text{Mem}}^{\text{CH}_3\text{OH}} \frac{c_{\text{aCL}}^{\text{CH}_3\text{OH}} - c_{\text{cCL}}^{\text{CH}_3\text{OH}}}{\delta_{\text{Mem}}} \tag{5}$$

Noting that the methanol EOD coefficient, $n_{\text{d}}^{\text{CH}_3\text{OH}}$, is an increasing function of methanol concentration (see Table 2), we see here that a lower aCL methanol concentration reduces both diffusion and EOD components of the methanol crossover.

It should be noted that due to the capillary-induced liquid flow in the porous media, there is a net transport of liquid from the anode flow channel towards the aCL; therefore the concentration gradients, as observed in Fig. 4, only imply the effect of the aTB on diffusive transport. Further, as illustrated in Fig. 2, due to the binary nature of the CH$_3$OH/H$_2$O mixture, if the concentration of CH$_3$OH goes down, the concentration of H$_2$O must necessarily go up. This,
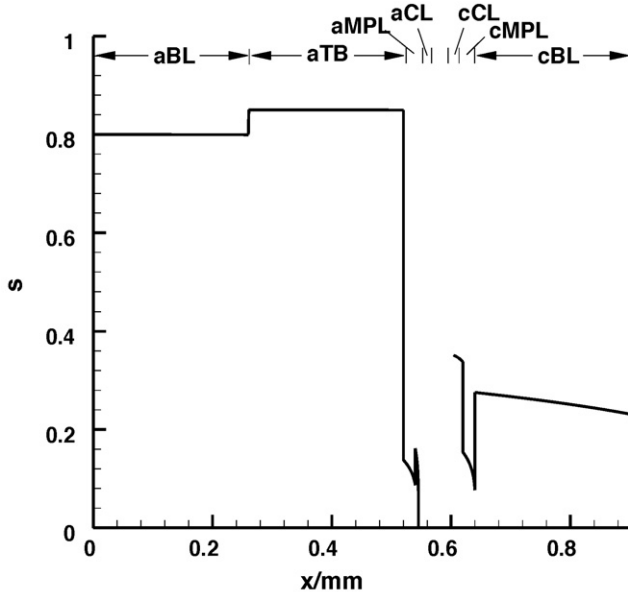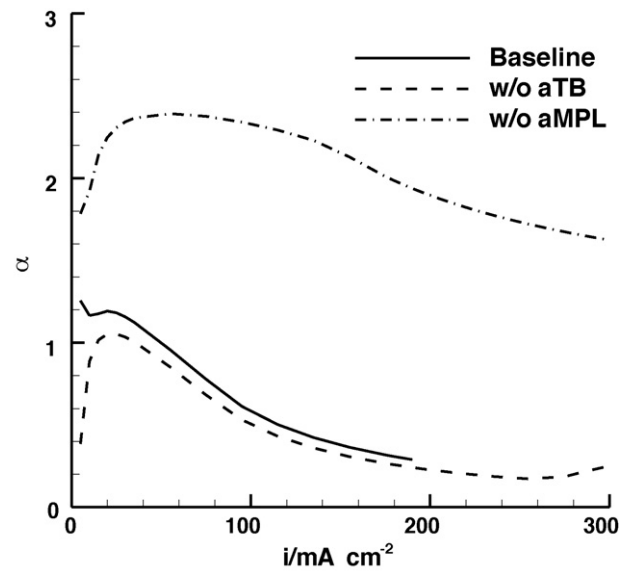

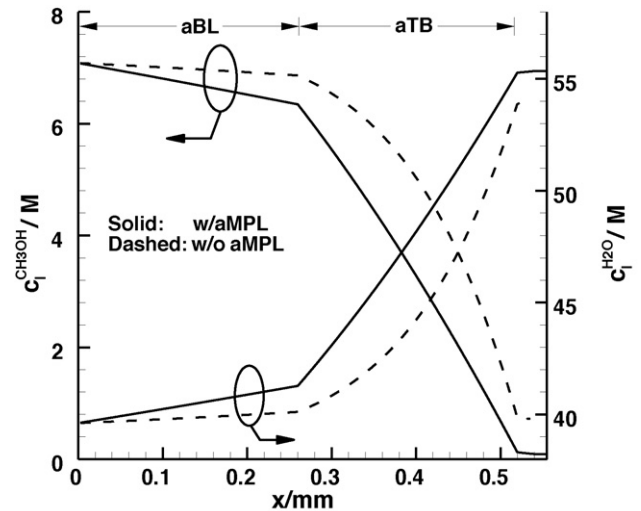**Fig. 7.** α vs. current density for baseline cell, baseline cell without aTB, and baseline cell without aMPL.

Fig. 8. Liquid CH$_3$OH and H$_2$O concentration profiles with and without hydrophobic aMPL; aTB present; i = 175 mA cm^{-2}.

Fig. 6. Anode and cathode liquid saturation profiles for baseline cell; i = 175 mA cm^{-2}.
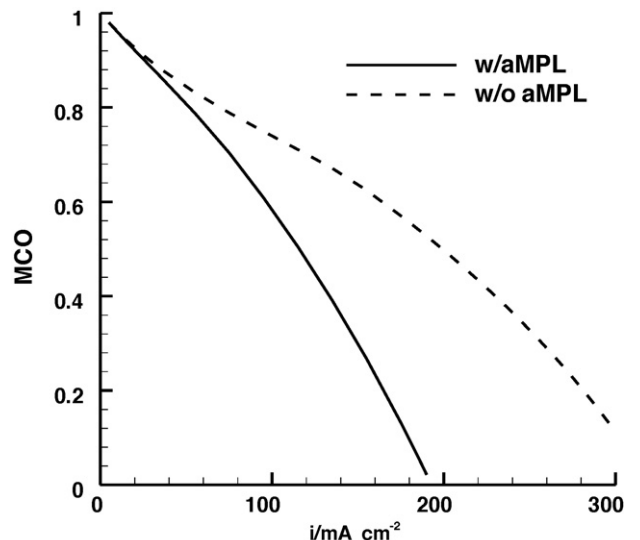

Fig. 9. MCO vs. current density with and without hydrophobic aMPL; aTB present.
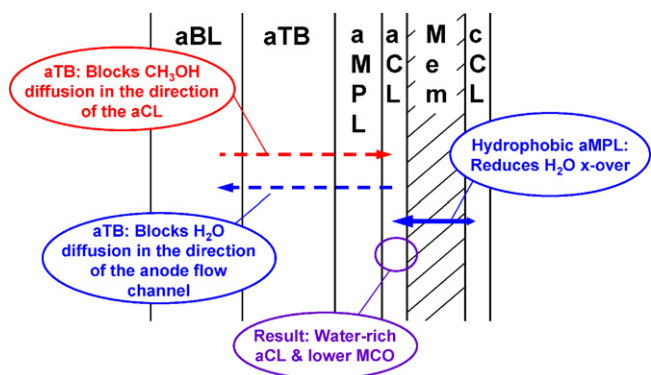
Fig. 10. Schematic of how the aTB and aMPL work together to create water-rich aCL.

of course means that any layer that acts as a barrier to methanol diffusion towards the aCL necessarily also acts as a barrier to H_2O diffusion towards the channel.

The liquid saturation profile for the baseline cell at an operating current density of 175 mA cm^{-2} is shown in Fig. 6. Note the high liquid saturation of $s \sim 0.85$ in the aTB region, as compared with $s \sim 0.8$ in the aBL. As we will elucidate further in the next section, properties that create this high liquid saturation level coupled with a low porosity ($\varepsilon = 0.25$, as listed in Table 1) are what make the aTB an

effective obstruction to diffusion. In this work, we approximate the effective diffusivity for the liquid and vapor phases with the Bruggeman correlation, which clearly highlights the liquid saturation and porosity effects:

$$D_{\mathrm{eff,l}}^{\psi_1,\psi_2} = D_{\mathrm{l}}^{\psi_1,\psi_2}[s\varepsilon]^n \qquad (6)$$

$$D_{\mathrm{eff,g}}^{\psi_1,\psi_2} = D_{\mathrm{g}}^{\psi_1,\psi_2}[(1-s)\varepsilon]^n \qquad (7)$$

All diffusivity values used are listed in Table 2, along with the Bruggeman exponent, which we assume to be $n = 2.1$. A low porosity directly reduces the effective diffusivity in both the liquid and gas phases. A higher liquid saturation level increases the liquid phase effective diffusivity and decreases the gas phase effective diffusivity. Because species transport can take place in either the liquid or gas phases, this shift in effective diffusivities essentially increases the resistance to diffusion transport in the gas phase and reduces it in the liquid phase. Seeing how the molecular diffusivity in the liquid phase is $\sim 10^{-9}$ m^2 s^{-1} compared with $\sim 10^{-5}$ m^2 s^{-1} in the gas phase, the ultimate effect of the greater liquid saturation is a greater overall resistance to transport via diffusion.

While the aTB facilitates the use of high concentration methanol fuel by hindering CH_3OH and H_2O diffusion between the flow channel and the aCL, it does not directly address the critical issue of membrane water transport and steady-state source of water supply into the aCL (see Fig. 1). As shown in Fig. 7, the inclusion of the
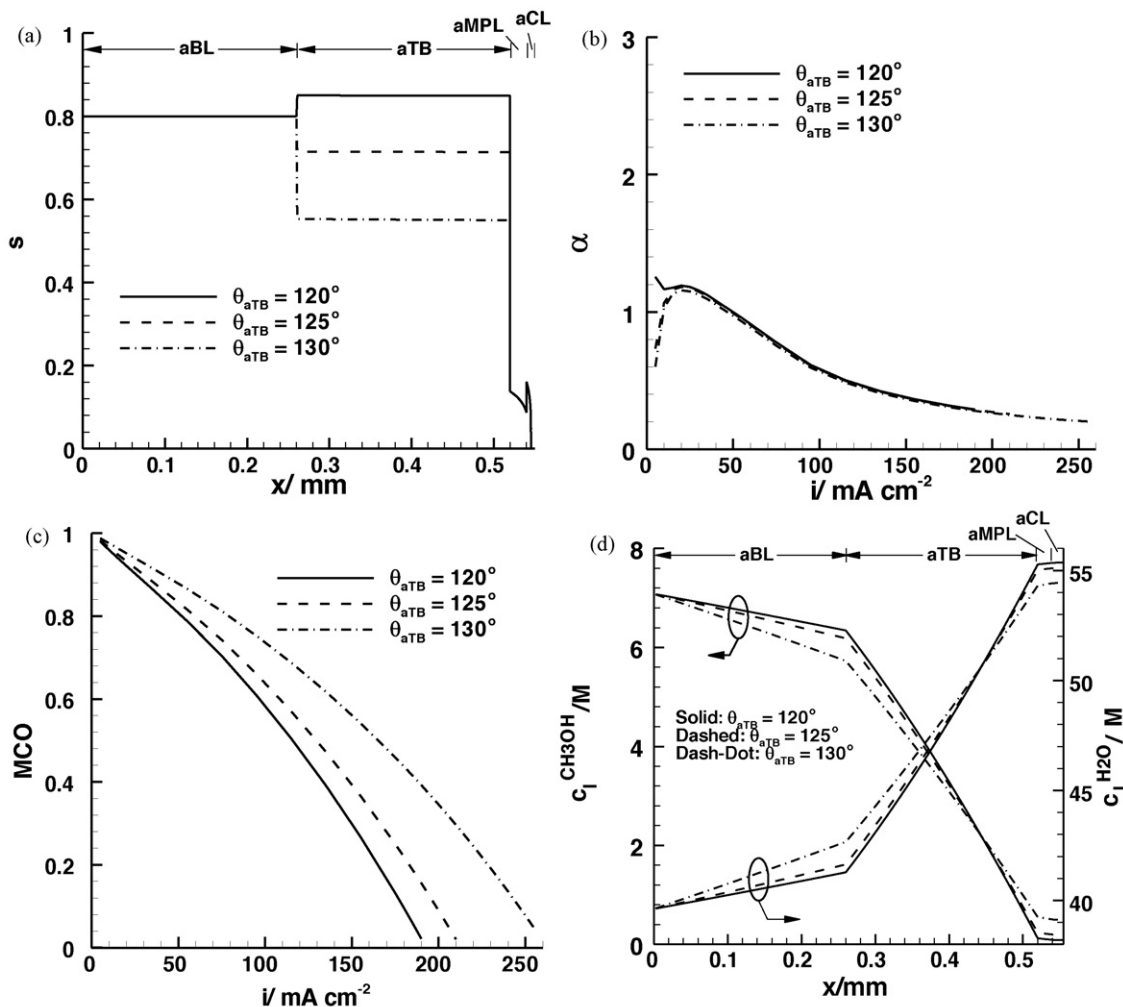

Fig. 11. Effect of aTB contact angle: (a) anode liquid saturation profiles at $i = 175$ mA cm^{-2}, (b) α vs. current density, (c) MCO vs. current density and (d) liquid CH_3OH and H_2O concentration profiles at $i = 175$ mA cm^{-2}.
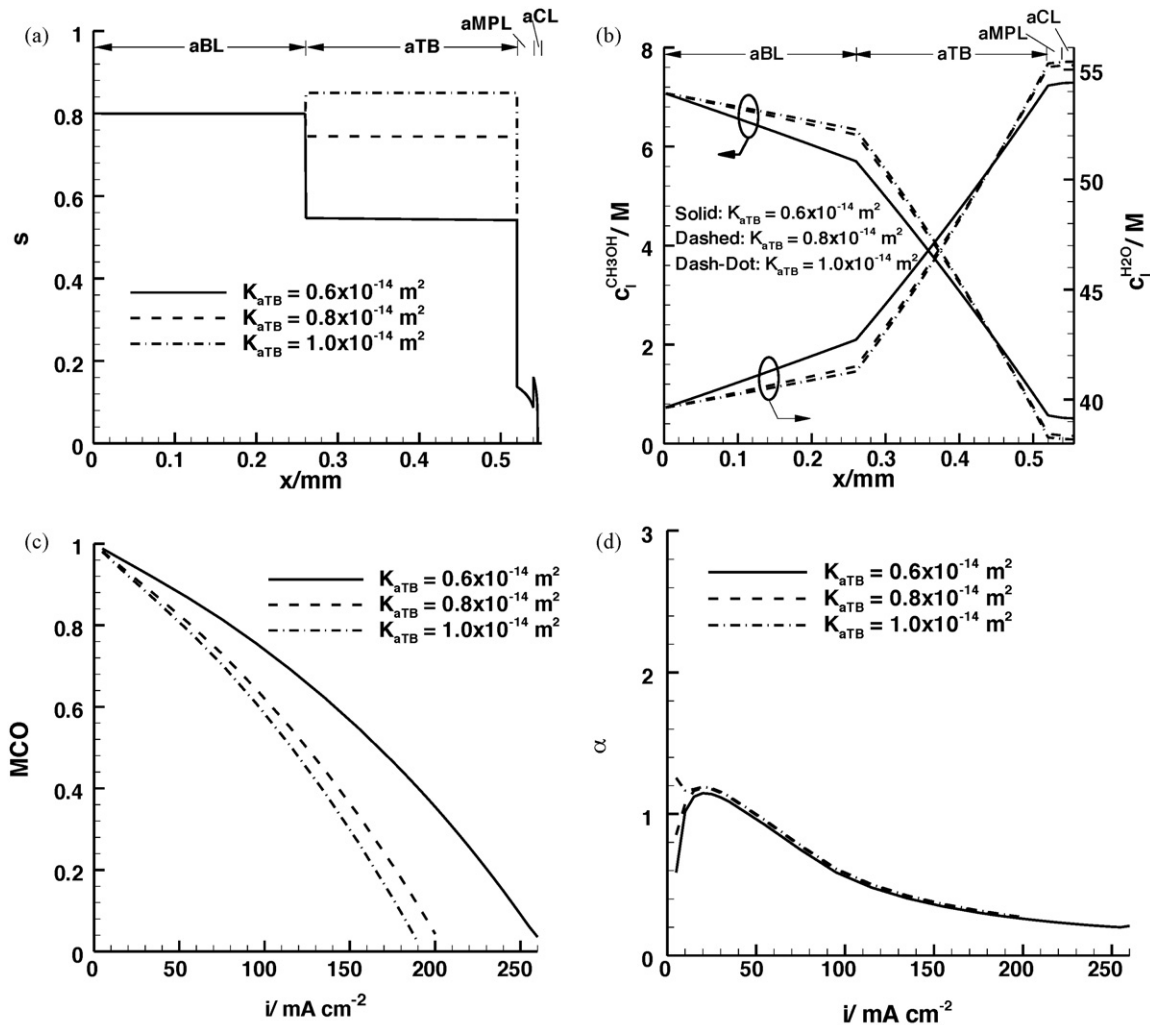
Fig. 12. Effect of aTB permeability: (a) anode liquid saturation profiles at $i = 175$ mA cm^{-2}, (b) liquid CH$_3$OH and H$_2$O concentration profiles at $i = 175$ mA cm^{-2}, (c) MCO vs. current density and (d) α vs. current density.

aTB actually slightly *increases* α. This is most likely due to the corresponding drastic increase in MCO without the aTB, which leads greater H$_2$O production in the cCL and hence more back-diffusion of H$_2$O leading to slightly lower α. However, from Fig. 7, we see that the hydrophobic aMPL is clearly the primary reason for low α in the baseline cell ($\alpha \sim 0.35$ with aMPL; $\alpha \sim 2.0$ without aMPL at 175 mA cm^{-2}). A more detailed physical explanation of exactly how the aMPL causes a lower α value is given in Section 3.3 after we introduce a few additional concepts (an even more rigorous explanation can be found in Refs. [10–15]). At this point, however, it is important to note that the lower α value with hydrophobic aMPL is primarily due to a lower liquid saturation level in the aCL with aMPL present.

Analyzing Figs. 8 and 9, we see that in addition to simply reducing α, the aMPL also makes the aTB more effective. Fig. 8 shows that the lower α realized by using an aMPL makes the aCL more water-rich, as the liquid H$_2$O concentration is higher, and the liquid methanol concentration is lower in the aCL with aMPL present. As discussed previously, this lower methanol concentration in the aCL leads to a reduction in methanol transport across the membrane due to a reduction in both EOD and diffusion. Fig. 9 further highlights this point by showing that a significantly lower MCO is realized over the entire current density range with aMPL present (e.g. at $i \sim 175$ mA cm^{-2}, MCO ~ 0.15 with aMPL; MCO ~ 0.57 without aMPL).

The underpinning concept to be take from Figs. 4–9 with regards to the direct use of high concentration methanol fuel is that the aTB and aMPL work *in conjunction* with one another. This is best summed up by the sketch given in Fig. 10, which highlights the aTB acting as a hindrance to diffusion of CH$_3$OH and H$_2$O between flow channel and aCL, while the aMPL essentially creates a source of water flowing into the aCL by reducing the amount of water crossing the membrane (low α). These two effects lead to a more water-rich aCL, and corresponding lower MCO.

3.2. Effect of aTB properties on α and MCO

The effect of variable aTB contact angle is shown in Fig. 11. As illustrated in Fig. 11(a), the main effect of an increasing aTB contact angle is to reduce the liquid saturation level within the aTB. However, as shown in Fig. 11(b), this increasing hydrophobicity has a very minimal effect on α, as there is no discernable difference for various aTB contact angles at operating current density ($\sim$175 mA cm^{-2}). It has been shown in Refs. [10–15], and further discussed in the next section, that a hydrophobic aMPL reduces α. This fact naturally begs the question, "Why does an increasing aMPL contact angle significantly reduce α, while an increasing aTB contact angle has such little effect on α?" The answer has to do with the relatively high liquid saturation level of $s \sim 0.5$ in the aTB even with $\theta_{aTB} = 130°$ (Fig. 11(a)); when compared with an aMPL
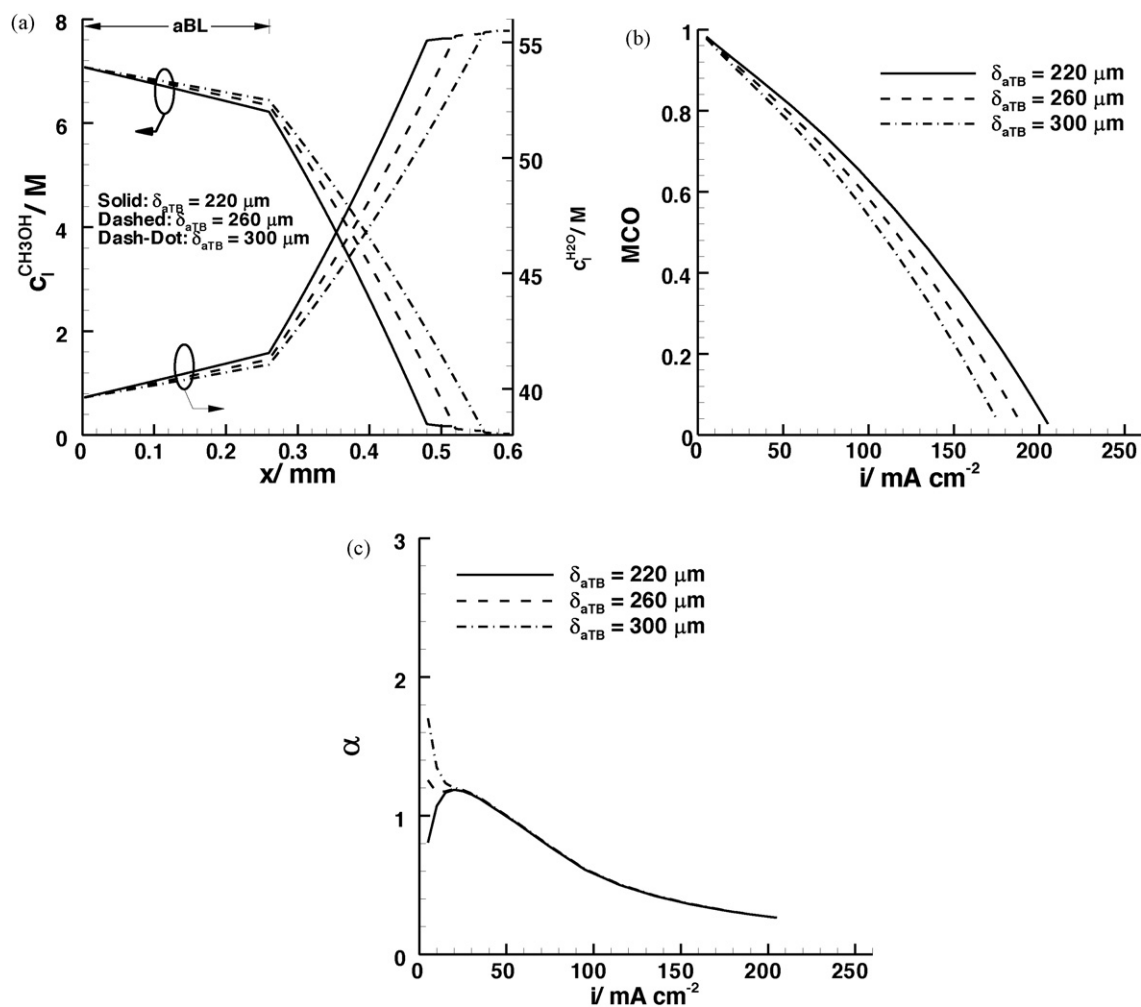
Fig. 13. Effect of aTB thickness: (a) liquid CH_3OH and H_2O concentration profiles at $i = 175$ mA cm^{-2}, (b) MCO vs. current density and (c) α vs. current density.

with the same contact angle, the aTB has higher liquid saturation level primarily due to differences in other assumed properties (see Table 1). As described in Refs. [10,11], in the 1D model we solve for the liquid saturation from the following equation (which comes from Darcy's law):

$$\frac{ds}{dx} = \left[\frac{M_l \mu_l}{\rho_l (K\varepsilon)^{1/2} (\sigma \cos \theta)(dJ/ds)} \right] \frac{N_l(x)}{k_{rl}} \quad (8)$$

Because the relative liquid-phase permeability, k_{rl}, is a strong function of the liquid saturation (see Table 2), for the same flux in the liquid phase, N_l, at lower values of s the gradient in liquid saturation will be much greater. Due to the fact that $s \sim 0.5$ in the aTB with $\theta_{aTB} = 130°$, there is little drop in liquid saturation level over the aTB, correspondingly little effect on the saturation level in the aCL, and ultimately little effect on α.

Fig. 11(c) illustrates that a higher aTB contact angle leads to a higher MCO. We see in Fig. 11(d) that this higher MCO with increasing contact angle is due to the aTB becoming a less effective barrier to methanol and H_2O diffusion. These results should come as no surprise in light of the contact angle effect on liquid saturation given in Fig. 11(a), and the physical explanation given previously of what makes an effective aTB. These results further imply that the most effective aTB may actually be hydrophilic, which would yield a layer with nearly 100% liquid saturation. Liu and Wang [14] noted that a hydrophilic aMPL (in an MEA without aTB), while causing a larger α, also reduced the limiting current density. This implies

that the hydrophilic aMPL was a greater barrier to methanol diffusion toward the aCL and H_2O back-diffusion, which is exactly the goal of the aTB. The authors [14] attributed this increased transport resistance to the porosity of a hydrophilic aMPL being lower than that of a similar PTFE-treated hydrophobic aMPL as a result of the former's swelling as a consequence of its Nafion® treatment. We theorize from the results of this work, that the effectiveness of a hydrophilic anode layer (aMPL or aTB) in being a barrier to CH_3OH forward and H_2O back-diffusion is due not only to a lower porosity, but also simply to its hydrophilic nature, and corresponding high liquid saturation level.

The effect of variable aTB permeability is shown in Fig. 12. In Fig. 12(a), we see that a larger aTB permeability leads to a higher liquid saturation level. Using the same logic as with the variable aTB contact angle, we see in Fig. 12(b) that this greater liquid saturation level leads to a more effective barrier to methanol and H_2O diffusion, highlighted by the larger methanol and H_2O gradients in the aTB. The greater resistance of course yields the lower MCO with greater aTB permeability, as shown in Fig. 12(c). Finally, Fig. 12(d) shows that a variable aTB permeability – at least in the range tested here – has little effect on α. By analyzing Fig. 12(a) and thinking once again with reference to Eq. (8), this minimal effect on α can be attributed to the liquid saturation level remaining relatively high in the aTB (even for $K_{aTB} = 0.6 \times 10^{-14}$ m^2, $s > \sim 0.5$ in the aTB).

Variable aTB thickness effect is illustrated in Fig. 13. It should come as no great surprise that a thicker aTB acts as a more effective barrier to methanol and H_2O diffusion, as highlighted in Fig. 13(a).
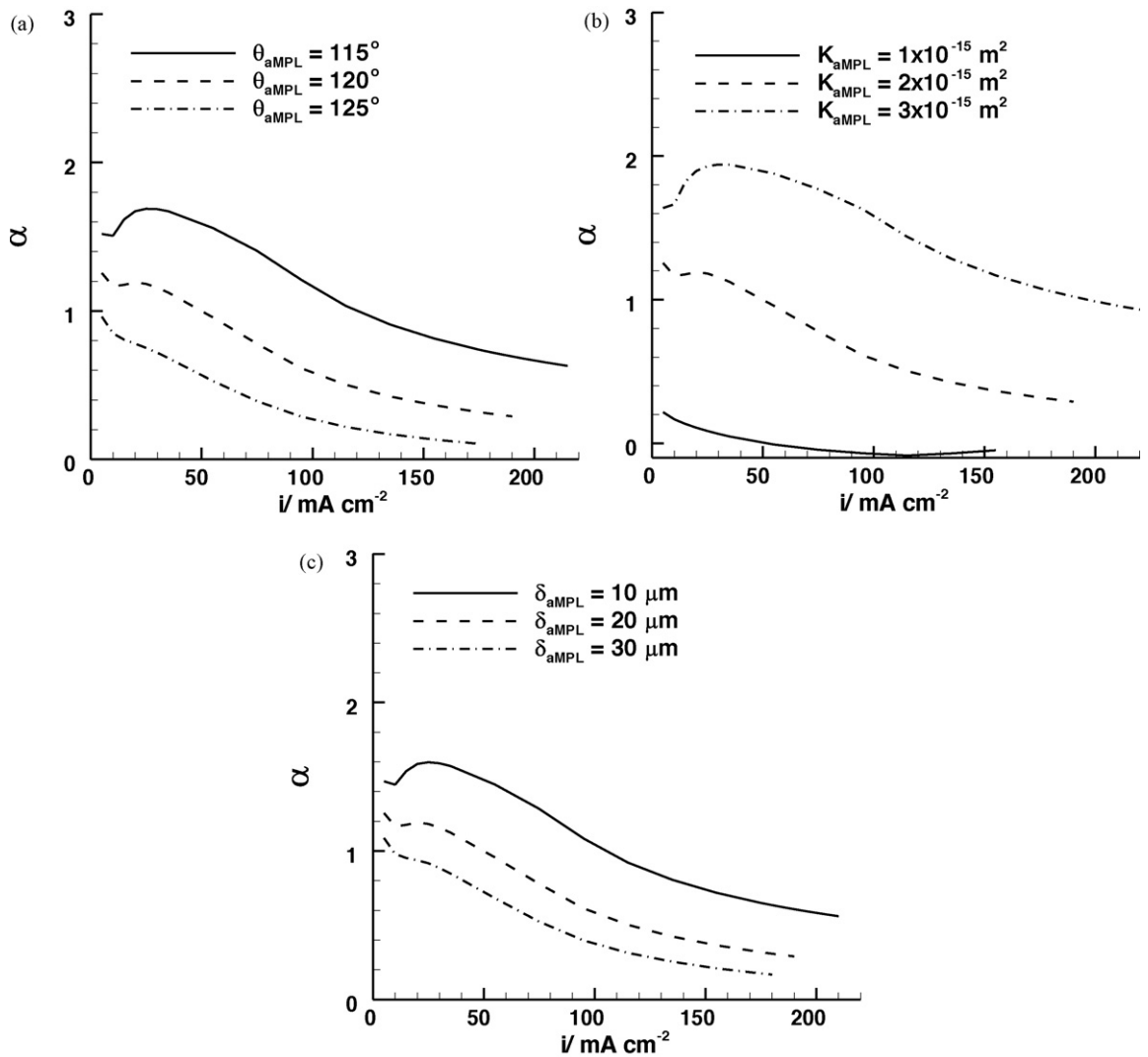
Fig. 14. α vs. current density for various (a) aMPL contact angles, (b) aMPL permeabilities and (c) aMPL thicknesses.

Naturally, this leads to a lower MCO with thicker aTB, as highlighted in Fig. 13(b). Finally, Fig. 13(c) shows that the varying aTB thickness has no discernable effect on α. This again should be expected by analyzing the saturation level given in Fig. 6, which shows that for the aTB properties modeled (Fig. 13 has baseline cell properties, but with variable aTB thickness), the liquid saturation remains at the relatively high level of $s \sim 0.85$.

3.3. Effect of aMPL properties on α and MCO

A detailed theory of how a hydrophobic aMPL reduces α in an MEA without aTB can be found in Refs. [10–15], and the same theory applies here with the aTB. To summarize briefly, due to its hydrophobic nature and low permeability, the aMPL has a low liquid saturation level, as evident in Fig. 6, where $s \sim 0.1$ in the aMPL for baseline parameters. With reference to Eq. (8), because of this low liquid saturation level, there is a large gradient in liquid saturation, resulting in a large drop in s across the aMPL (i.e. a large drop in liquid pressure). Ultimately, this leads to a lower liquid saturation level in the aCL with the aMPL present. We should note that in order to limit MCO to a tolerably low level under load (using any readily-available membrane, e.g. Nafion®), the CH$_3$OH concentration in the aCL must be kept low («1 M in our calculations), yielding a liquid in the aCL which is nearly all water. It has been shown that the mem-

brane water content, which drives H$_2$O membrane diffusion, and H$_2$O EOD drag coefficient are both much higher for a membrane in contact with liquid H$_2$O rather than vapor (see Table 2). Therefore, the effect of the lower aCL liquid saturation is ultimately a greater back-diffusion and lower EOD of H$_2$O, yielding a lower α value.

The parametric effect of aMPL contact angle, permeability, and thickness on α and MCO are summarized in Figs. 14 and 15, respectively. In Fig. 14 we see that an aMPL with greater contact angle (i.e. more hydrophobic), smaller permeability, and greater thickness reduces α. It is further evident from Fig. 15 that these same parameters that reduce α also result in a slight reduction of MCO. The reduction in methanol crossing the membrane is a direct consequence of the dilution effect of low α on the methanol concentration in the aCL.

3.4. Determining most efficient fuel concentration for HC-MFC

In this section, we turn our attention to determining the most efficient fuel concentration to carry in the fuel tank as part of a DMFC system design. By "most efficient" here, we mean the most efficient use of system volume, weight, etc., as the goal is to minimize or eliminate the need to carry excess H$_2$O or CH$_3$OH in the system, all while utilizing only internal water management. We will assume that our MEA is designed with baseline aTB, and base-
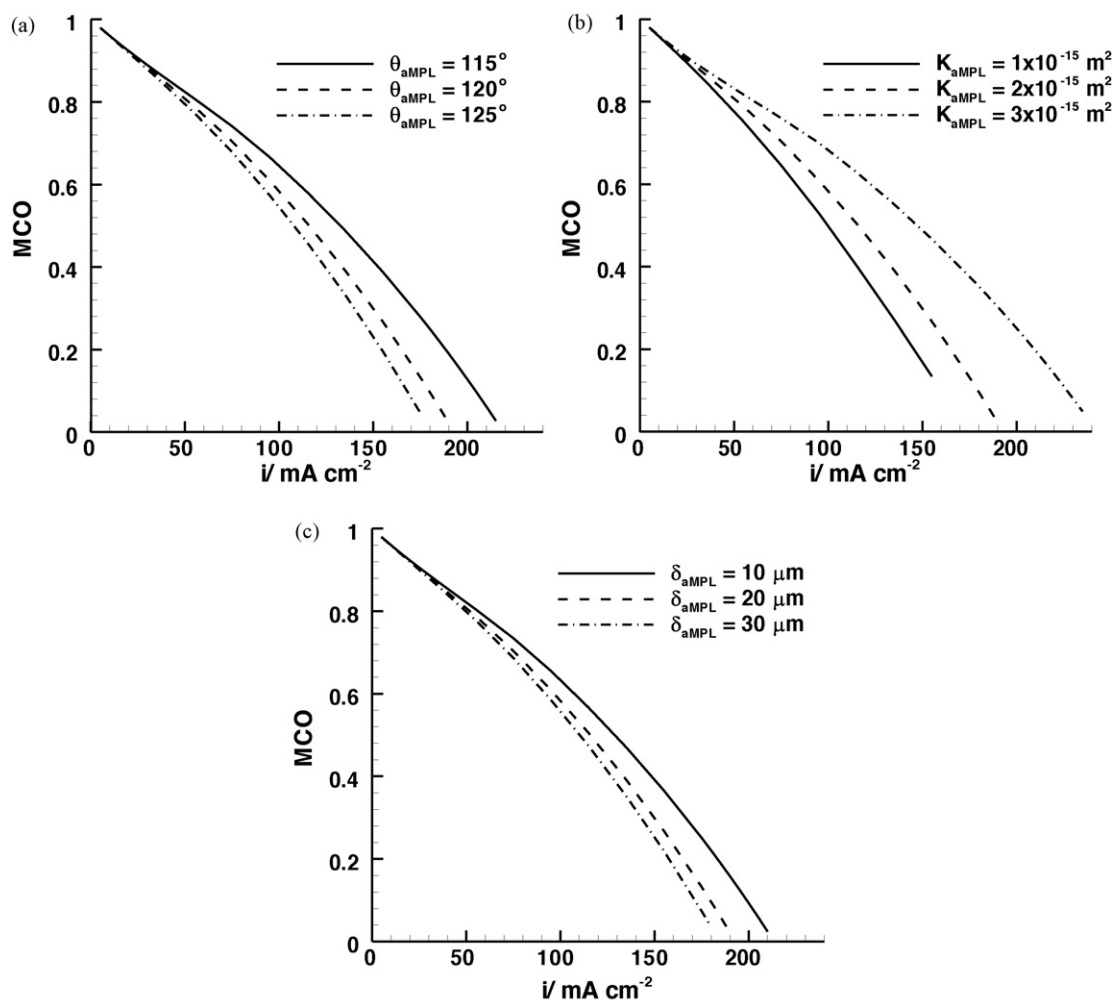
Fig. 15. MCO vs. current density for various (a) aMPL contact angles, (b) aMPL permeabilities and (c) aMPL thicknesses.

line aMPL properties, but with a thickness of 30 μm in effort to reduce α. A typical operating condition for a DMFC is at a current density of $\sim$80–90% of the limiting current density (i.e. just before the mass transport limiting region); this operating point typically yields a reasonable tradeoff between good performance (voltage or power), and high fuel efficiency (low MCO). At this operating point, MCO is typically $\sim$0.2 for a well-designed MEA, so we will use MCO = 0.2 in this example as our design point criteria.

The MCO = 0.2 curve in Fig. 1 will serve as the guide for choosing a fuel concentration which yields optimal use of our system volume, for a DMFC utilizing the prescribed MEA. This process is iterative, as we do not know what α value the simulated MEA will yield *a priori*, and because α is also a function of the fuel concentration used. However, as α is primarily determined by aMPL properties, from Fig. 14, we can hypothesize that this MEA will yield $\alpha \sim 0.2$. Looking at the MCO = 0.2 curve at $\alpha \sim 0.2$ in Fig. 1, we find a corresponding fuel concentration of $\sim$14 M, which is the value that we will choose for our first simulation. Table 3 shows the results of this simulation at

Table 3
Iterations for determining the most efficient fuel concentration for MEA with baseline aTB and baseline aMPL but with 30 μm thickness.

Iteration	Fuel concentration, $c_o^{CH_3OH}$ (M)	Simulated i at MCO = 0.2 (mA cm^{-2})	Simulated α at MCO = 0.2
1	14	201.75	0.137
2	14.5	206.75	0.131

MCO = 0.2, listed as iteration 1. We see from this data that the actual α value corresponding to 14 M fuel is $\alpha = 0.137$, meaning that our initial guess was fairly accurate. Turning our attention once again to Fig. 1, we see that $\alpha = 0.137$, the optimal fuel concentration is actually closer to 14.5 M, and therefore make a second simulation at this value. Table 3 illustrates that for $c_o^{CH_3OH} = 14.5$ M, $\alpha = 0.131$ for MCO = 0.2; for our purposes, this is clearly accurate enough, as the $c_o^{CH_3OH} = 14.5$ M, $\alpha = 0.131$ point essentially lies on the MCO = 0.2 curve in Fig. 1. This means that the proposed MEA design will allow us to directly use $\sim$14.5 M fuel in an energy dense DMFC system, while operating at a fuel efficiency of $\sim$80%, without any external means of water recovery!

4. Conclusions

A primary focus of current DMFC research is on designing an MEA that allows the efficient and direct use of highly concentrated methanol fuel. Because H_2O and CH_3OH react 1:1 (on a molar basis) in the aCL, realizing a low water crossover to the cathode is a necessary prerequisite of any such MEA. Designing this type of MEA will lead to a more energy dense DMFC system, and allow DMFCs to be more competitive with Li-ion batteries. In this work we have presented a novel MEA design – an extension of the traditional low-α MEA – in which we utilize an anode transport barrier between backing layer and hydrophobic anode MPL. It has been shown that the primary role of the aTB is to block methanol and water diffusion between the methanol-rich fuel feed and the water-rich aCL; the

primary role of the hydrophobic aMPL is to reduce the net water transport into the cathode. We have further elucidated how these two roles of the aTB and aMPL work together to form an MEA which yields a low water and methanol crossover, while directly operating on highly concentrated methanol fuel.

It has been shown that a thicker aTB with smaller contact angle (i.e. more hydrophilic), and higher permeability is most effective in reducing the methanol crossover to the cathode. In fact the results given in this work lead us to believe that the most effective aTB may actually be hydrophilic. A thicker, more hydrophobic (larger contact angle), less permeable aMPL was found to be most effective in reducing α, which is the same conclusion reached by Liu and Wang [14,15] and Shaffer and Wang [10–13] for an MEA without aTB operating on low concentration methanol fuel. Finally, this work presents a theory of how and why the proposed MEA design is successful in its stated goals, a theory that hopefully can aid future novel MEA and DMFC designs.

Acknowledgements

References

[1] C.K. Dyer, J. Power Sources 106 (2002) 31.
[2] S. Gottesfeld, in: A.J. Bard, M. Stratmann, D.D. Macdonald, P. Schmuki (Eds.), Encyclopedia of Electrochemistry, vol. 5, Wiley-VCH Verlag GmbH & Co. KGaA, Weinheim, 2007, p. 3 (Chapter 8).
[3] C.Y. Wang, Chem. Rev. 104 (2004) 4727.
[4] G. Lu, C.Y. Wang, in: B. Sunden, M. Faghri (Eds.), Transport Phenomena in Fuel Cells (Developments in Heat Transfer), vol. 19, WIT Press, Boston, 2004 (Chapter 9).
[5] S.K. Kamarudin, W.R.W. Daud, S.L. Ho, U.A. Hasran, J. Power Sources 163 (2007) 743.
[6] G.Q. Lu, F.Q. Liu, C.Y. Wang, Electrochem. Solid-State Lett. 8 (2005) A1.
[7] F. Liu, G. Lu, C.Y. Wang, J. Electrochem. Soc. 153 (2006) A543.
[8] C.Y. Wang, F. Liu, Proceedings of the 8th Small Fuel Cell Symposium, Washington, DC, April, 2006 (Chapter 10).
[9] A. Blum, T. Duvdevani, M. Philosoph, N. Rudoy, E. Peled, J. Power Sources 117 (2003) 22.
[10] C.E. Shaffer, C.Y. Wang, Electrochim. Acta 54 (2009) 5761.
[11] C.E. Shaffer, C.Y. Wang, Proceedings of the 6th International Fuel Cell Science Engineering and Technology Conference, Denver, CO, USA, 16–18 June, 2008.
[12] C.E. Shaffer, C.Y. Wang, ECS Trans. 16 (2008) 1507.
[13] C.E. Shaffer, C.Y. Wang, in: W. Vielstich, H. Yokokawa, H.A. Gasteiger (Eds.), Handbook of Fuel Cells, vol. 6, Wiley, Chichester, UK, 2009, p. 749.
[14] F. Liu, C.Y. Wang, Electrochim. Acta 53 (2008) 5517.
[15] F.Q. Liu, Ph.D. Thesis, The Pennsylvania State University, University Park, Pennsylvania, 2006.
[16] F.Q. Liu, C.Y. Wang, Electrochem. Solid State Lett. 12 (2009) B101.
[17] C.Y. Wang, G. Lu, W. Liu, F. Liu, Y. Sato, E. Sakaue, K. Matsuoka, U.S. Patent Pub. No. US 2006/0134487 A1 (2006).
[18] X. Ren, F.W. Kovacs, K.J. Shufon, S. Gottesfeld, U.S. Patent Pub. No. US 2004/0209154 A1 (2004).
[19] C. Lim, C.Y. Wang, J. Power Sources 113 (2003) 145.
[20] C.Y. Wang, F. Liu, Y. Sato, E. Sakaue, U.S. Patent Pub. No. US 2007/0087234 A1 (2007).
[21] F. Liu, C.Y. Wang, J. Electrochem. Soc. 154 (2007) B514.
[22] K.Y. Song, H.K. Lee, H.T. Kim, J. Electrochim. Acta 53 (2007) 637.
[23] J.Y. Park, J.H. Lee, S.K. Kang, J.H. Sauk, I. Song, J. Power Sources 178 (2008) 181.
[24] U. Pasaogullari, C.Y. Wang, J. Electrochem. Soc. 151 (2004) A399.
[25] W. Liu, Ph.D. Thesis, The Pennsylvania State University, University Park, Pennsylvania, 2005.
[26] U. Pasaogullari, C.Y. Wang, Electrochim. Acta 49 (2004) 4359.
[27] J.H. Nam, M. Kaviany, Int. J. Heat Mass Transfer 46 (2003) 4595.
[28] R.H. Brooks, A.T. Corey, Hydrology Papers, Colorado State University 3 (1964).
[29] R.B. Mrazek, C.E. Wicks, K.N.S. Prabhu, J. Chem. Eng. Data 13 (1968) 508.
[30] B.E. Poling, J.M. Prausnitz, J.P. O'Connell, The Properties of Gases and Liquids, 5th ed., McGraw-Hill, New York, 2001.
[31] Z.J. Derlacki, A.J. Easteal, V.J. Edge, L.A. Woolf, Z. Roksandic, J. Phys. Chem. 89 (1985) 5318.
[32] T.A. Zawodzinski, C. Derouin, S. Radzinski, R.J. Sherman, V.T. Smith, T.E. Springer, S. Gottesfeld, J. Electrochem. Soc. 140 (1993) 1041.
[33] T.E. Springer, T.A. Zawodzinski, S. Gottesfeld, J. Electrochem. Soc. 138 (1991) 2334.
[34] T.A. Zawodzinski, J. Davey, J. Valerio, S. Gottesfeld, Electrochim. Acta 40 (1995) 297.
[35] W. Liu, C.Y. Wang, J. Electrochem. Soc. 154 (2007) B352.
[36] M.L. McGlashan, A.G. Williamson, J. Chem. Eng. Data 21 (1976) 196.